crystals

MDPI

Article

A Linear Regression Model for Determining the Pre-Exponential Factor and Interfacial Energy Based on the Metastable Zone Width Data

Lie-Ding Shiau [1,2]

[1] Department of Chemical and Materials Engineering, Chang Gung University, Taoyuan 333, Taiwan; shiau@mail.cgu.edu.tw; Tel. +011-886-3-211-8800 (ext. 5291); Fax. +011-886-3-2118700

[2] Department of Urology, Chang Gung Memorial Hospital Linkou, Taoyuan 333, Taiwan

Received: 8 January 2020; Accepted: 7 February 2020; Published: 11 February 2020

Abstract: A linear regression model is presented in this study to determine the pre-exponential factor and interfacial energy of the crystallized substance based on classical nucleation theory using the metastable zone width data. The nucleation event is assumed corresponding to a point at which the total number density of the nuclei has reached a fixed (but unknown) value. One equation is derived for any temperature-dependent functional form of the solubility. Another equation is derived for the van't Hoff solubility expression. The pre-exponential factor and interfacial energy obtained from these two equations are found consistent for the studied systems, including glutamic acid, glycine, and 3-nito-1,2,4-triazol-5-one. The results obtained from these two equations are also compared with those obtained from the integral method and classical 3D nucleation theory approach.

Keywords: crystallization; nucleation; metastable zone width; pre-exponential factor; interfacial energy

1. Introduction

The nucleation behavior in a supersaturated solution is closely related to the induction time or metastable zone width (MSZW) measurements [1–3]. As opposed to a lag time during the temperature-decreasing process for the prepared supersaturated solution at a higher temperature lowered to the desired constant temperature in the induction time measurements, there is no lag time for the supersaturated solution cooled at a constant cooling rate in the MSZW measurements. Thus, the MSZW data should be more reliable than the induction time data in determination of the nucleation rate for a system.

In classical nucleation theory (CNT) [1–3], the nucleation rate of a crystallization system depends on both the pre-exponential factor and interfacial energy, which are usually determined using induction time data by assuming $J \propto {t_i}^{-1}$, where J is the nucleation rate and t_i is the induction time [4–10]. Due to the complicated data interpretation method, determination of the pre-exponential factor and interfacial energy using MSZW data has long been a challenging task.

Based on the Nyvlt's approach [11,12], Sangwal [13–16] proposed a self-consistent Nyvlt-like equation using the power-law nucleation rate, leading to a linear relationship between $\ln\left(\frac{\Delta T_m}{T_0}\right)$ and lnb, where T_0 is the initial saturated temperature, ΔT_m is the MSZW, and b is the cooling rate. Similarly, using the nucleation rate based on CNT, Sangwal [13–16] developed a linear relationship of $\left(\frac{T_0}{\Delta T_m}\right)^2$ versus lnb. Kashchiev et al. [17] presented a general expression for the total volume and number of crystallites as functions of the cooling rate for progressive nucleation based on CNT. They

verified that the linear dependence of $\ln\left(\frac{\Delta T_m}{T_0}\right)$ on lnb is the linear approximation to their presented equation. For instantaneous nucleation, a more simplified model is derived by Kashchiev et al. [18] which also yields a linear relationship between $\ln\left(\frac{\Delta T_m}{T_0}\right)$ and lnb. Kubota [19] proposed a model based on progressive nucleation to account for the MSZW limit corresponding to a point at which the number density of accumulated crystals has reached a fixed (but unknown) value during the cooling process. The simple power-law form of nucleation rate is adopted in the Kubota's model, leading to a linear relationship of $\ln \Delta T_m$ versus lnb for the MSZW data.

The above-mentioned models have been widely applied in the literature to correlate MSZW with cooling rate in various crystallization systems [20–27]. Although the pre-exponential factor and interfacial energy can provide important information in understanding the nucleation behavior, the pre-exponential factor and interfacial energy of the crystallized substance are usually not determined in these studies. Recently, some researchers [28–30] investigated the relationship between MSZW and process parameters in terms of the pre-exponential factor and interfacial energy using classical 3D nucleation theory approach based on the Sangwal's theory [13–16]. Shiau and Lu [31–33] developed an integral model to determine the pre-exponential factor and interfacial energy based on CNT using the MSZW data. As the nonlinear regression along with numerical integration involved in the integral model is complicated, the objective of this work is to present a linear regression model to determine the pre-exponential factor and interfacial energy of the crystallized substance based on CNT using the MSZW data.

2. Theory

2.1. Integral Method

The nucleation rate based on CNT is expressed as [1–3]

$$J = A_J exp\left[-\frac{16\pi v^2\gamma^3}{3{k_B}^3T^3ln^2S}\right] \quad (1)$$

Where A_J is the nucleation pre-exponential factor, γ is the interfacial energy, k_B is the Boltzmann constant, and $v = \frac{M_W}{\rho_c N_A}$ is the molecular volume.

To interpret the onset of nucleation based on the progressive nucleation observed in the induction time and MSZW measurements, the nucleation event is assumed corresponding to a point at which the total number density of the nuclei has reached a fixed (but unknown) value, f_N [19,30–32]. Thus, one can derive $f_N = J\, t_i$ at the induction time, which is consistent with $J \propto {t_i}^{-1}$ reported in the literature [1]. As nuclei are continuously born during the cooling process, Shiau and Lu [31–33] derived at the MSZW limit:

$$f_N = \int_0^{t_m} J\ dt \quad (2)$$

where f_N depends on the measurement device and on the substance.

If the solution is cooled at a constant rate defined as:

$$b = -dT/dt\ \ (b > 0) \quad (3)$$

one obtains $T(t) = T_0 - bt$ during the cooling process. Substituting Equations (1) and (3) into Equation (2) yields [31–33]:

$$\frac{f_N}{A_J} = -\int_{T_0}^{T_m} exp\left[-\frac{16\pi {v_m}^2\gamma^3}{3{k_B}^3T^3ln^2S}\right]\frac{dT}{b} \quad (4)$$

where, as shown in Figure 1, T_0 is the initial saturated temperature at $t = 0$, T_m is the maximum supercooling temperature at t_m, $\Delta T_m = T_0 - T_m$ is the MSZW, C_0 is the saturated concentration at

T_0, $S(T) = \frac{C_0}{C_{eq}(T)}$ is the temperature-dependent supersaturation during the cooling process, and $C_{eq}(T)$ is the temperature-dependent solubility. Note that C_0 remains unchanged before the onset of nucleation. As $C_{eq}(T)$ usually decreases with decreasing temperature, $S(T)$ increases with decreasing temperature; and subsequently J defined in Equation (1) increases during the cooling process.

Shiau and Lu [31–33] proposed the following nonlinear regression procedure to determine two parameters, γ and $\frac{A_J}{f_N}$, in Equation (4) from the experimental data of T_m versus b: (a) Guess γ; (b) determine $(\frac{A_J}{f_N})_j$ for each pair of T_m versus R data by numerical integration; (c) calculate $(\frac{A_J}{f_N})_{av}$; (d) calculate the coefficient of variation (CV) among all $(\frac{A_J}{f_N})_j$. For the guessed γ, $(\frac{A_J}{f_N})_{av}$ is defined as:

$$(\frac{A_J}{f_N})_{av} = \frac{1}{H}\sum_{j=1}^{H}(\frac{A_J}{f_N})_j \tag{5}$$

where H is the number of data points $(H \geq 2)$. For the guessed γ, CV among all $(\frac{A_J}{f_N})_j$ is defined as:

$$CV = \frac{\sqrt{\frac{1}{H-1}\Sigma_{j=1}^{H}\left[(\frac{A_J}{f_N})_j - (\frac{A_J}{f_N})_{av}\right]^2}}{\left(\frac{A_J}{f_N}\right)_{av}} \tag{6}$$

The same procedure from (a) to (d) is repeated by guessing various values of γ until the optimal γ with the minimum CV is found. Then, the corresponding $(\frac{A_J}{f_N})_{av}$ calculated from the optimal γ is taken as the optimal $\frac{A_J}{f_N}$. If f_N is known, A_J can be determined.

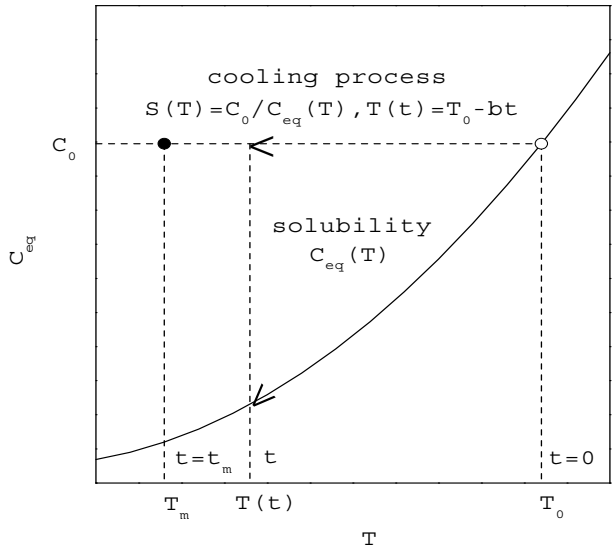

Figure 1. A schematic diagram showing the increasing of supersaturation during the cooling process for the saturated concentration C_0 (○ represents the starting point and • represents the nucleation point at a given b).

2.2. Linearized Integral Method

As the nonlinear regression along with numerical integration involved in Equation (4) is complicated, a simplified linear regression model is proposed in this study to extend the applicability of integral model as follows. Based on the trapezoidal rule for the numerical integration, Equation (2) is approximated as:

$$\frac{\Delta T_m}{2b}(J_0 + J_m) = f_N \tag{7}$$

Here, $\frac{\Delta T_m}{b}$ represents the total time required during the cooling process from T_0 to T_m at a constant cooling rate b. J_0 and J_m represent the nucleation rate at $t = 0$ and $t = t_m$, respectively. Note that $J_0 = 0$ due to $S(T_0) = \frac{C_0}{C_{eq}(T_0)} = 1$.

As shown in Figure 1, S increases gradually from 1 at $C_{eq}(T_0) = C_0$ during the cooling process. As defined in Equation (1), J starts from $J_0 = 0$ at $t = 0$ and increases gradually as temperature decreases from T_0 to T_m. The nucleation rate J_m at t_m can be expressed as:

$$J_m = A_J exp\left[-\frac{16\pi v^2\gamma^3}{3{k_B}^3{T_m}^3 ln^2 S_m}\right] \tag{8}$$

with

$$S_m = \frac{C_0}{C_m} \tag{9}$$

where $C_m = C_{eq}(T_m)$ is the saturated concentration at T_m and $S_m = S_m(T_m)$ is the supersaturation at T_m.

Substituting Equation (8) into Equation (7) yields:

$$exp\left[-\frac{16\pi v^2\gamma^3}{3{k_B}^3{T_m}^3 ln^2 S_m}\right] = \frac{2bf_N}{\Delta T_m A_J} \tag{10}$$

Taking logarithm on both sides of Equation (10) gives:

$$-\frac{16\pi v^2\gamma^3}{3{k_B}^3{T_m}^3 ln^2 S_m} = ln[\frac{2bf_N}{\Delta T_m A_J}] \tag{11}$$

By rearranging Equation (11), the linearized integral method I is expressed as:

$$\frac{1}{{T_m}^3 ln^2 S_m} = \frac{3}{16\pi}\left(\frac{{k_B}^3}{v^2\gamma^3}\right)\left[ln\left(\frac{\Delta T_m}{b}\right) + ln\left(\frac{A_J}{2f_N}\right)\right] \tag{12}$$

A plot of $\frac{1}{{T_m}^3 ln^2 S_m}$ versus $\ln\left(\frac{\Delta T_m}{b}\right)$ at a given T_0 should give a straight line, the slope and intercept of which permit determination of γ and $\frac{A_J}{f_N}$, respectively, without the knowledge of f_N.

If the temperature-dependent solubility is described in terms of the van't Hoff equation [1], one obtains:

$$\ln S_m = \ln\left(\frac{C_0}{C_m}\right) = \frac{-\Delta H_d}{R_G}(\frac{1}{T_0} - \frac{1}{T_m}) = (\frac{\Delta H_d}{R_G T_0})(\frac{\Delta T_m}{T_m}) \tag{13}$$

where ΔH_d is the heat of dissolution and R_G is the gas constant. By substituting Equation (13) into Equation (12), linearized integral method II is expressed as:

$$\frac{1}{T_m}(\frac{T_0}{\Delta T_m})^2 = \frac{3}{16\pi}(\frac{{k_B}^3}{v^2\gamma^3})(\frac{\Delta H_d}{R_G})^2[ln\left(\frac{\Delta T_m}{b}\right) + ln\left(\frac{A_J}{2f_N}\right)] \tag{14}$$

Similarly, a plot of $\frac{1}{T_m}(\frac{T_0}{\Delta T_m})^2$ versus $\ln\left(\frac{\Delta T_m}{b}\right)$ at a given T_0 should give a straight line, the slope and intercept of which permit determination of γ and $\frac{A_J}{f_N}$, respectively, without the knowledge of f_N.

It should be noted in the application of Equations (12) and (14) that γ is not influenced by the chosen value of f_N although A_J needs to be determined based on f_N. Based on the study of 28

inorganic systems, Mersmann and Bartosch [34] concluded that the minimum detectable volume fraction of nuclei in solution corresponds to $f_V = 10^{-4} - 10^{-3}$ with the minimum detectable size of $10 - 100\ \mu m$. The intermediate value, $f_V = 4 \times 10^{-4}$, was adopted at the detection of the nucleation point for the Lasentec focus beam reflectance measurements reported by Lindenberg and Mazzotti [35] and for the turbidity measurements reported by Shiau et al. [31–33,36]. If the uniform-sized spherical nuclei of $10\ \mu m$ with $k_V = \frac{\pi}{6}$ are assumed for simplicity, $f_V = 4 \times 10^{-4}$ corresponds to $f_N = 7.64 \times 10^{11}\ m^{-3}$ [32].

2.3. Classical 3D Nucleation Theory Approach

Sangwal [13–16] related J_m with the rate of change of solution supersaturation as:

$$J_m = f\frac{\Delta C}{C_m \Delta t} \tag{15}$$

where $\Delta C = C_0 - C_m$, $\Delta t = t_m$, and f is a constant defined as the number of clusters per unit volume. The value of f is governed by the aggregation and diffusion processes in the solution.

If S_m is slightly greater than 1, one obtains:

$$\ln S_m \cong S_m - 1 \tag{16}$$

Combining Equations (13) and (16) yields:

$$S_m - 1 = (\frac{\Delta H_d}{R_G T_0})(\frac{\Delta T_m}{T_m}) \tag{17}$$

Substituting Equation (9) into Equation (17) gives:

$$\frac{\Delta C_m}{\Delta T_m} = (\frac{\Delta H_d}{R_G T_0})(\frac{C_m}{T_m}) \tag{18}$$

By combining Equations (8), (15) and (18), Sangwal [13–16] derived the classical 3D nucleation theory approach as:

$$\left(\frac{T_0}{\Delta T_m}\right)^2 = F(1 - Z ln b) \tag{19}$$

Where:

$$Z = -1/ln(\frac{f\Delta H_d}{A_J R_G T_0 T_m}) \tag{20}$$

$$F = \frac{1}{Z}[\frac{3}{16\pi}(\frac{k_B T_0}{v^{2/3}\gamma})^3 \left(\frac{\Delta H_d}{R_G T_0}\right)^2] \tag{21}$$

A plot of $\left(\frac{T_0}{\Delta T_m}\right)^2$ versus $ln b$ at a given T_0 should give a straight line, the slope and intercept of which permit determination of Z and F, respectively. Subsequently, the values of γ and $\frac{A_J}{f}$ can be calculated without the knowledge of f.

It should be noted in the application of Equation (19) that γ is not influenced by the chosen value of f although A_J needs to be determined based on f. Sangwal [14] proposed that the upper limit of f may be estimated from solute concentration in the saturated solution. For example, $C_0 = 230\ kg\ /m^3$, the saturated concentration for aqueous glycine solutions at 308.15 K ($M_w = 0.075\ kg/mole$), corresponds to $C_0 = 1.84 \times 10^{27}\ m^{-3}$ based on the number of solute molecules per unit solution volume, which is close to $f = 10^{27}\ m^{-3}$ proposed by Sangwal [14].

3. Results and Discussion

The experimental MSZW data for three crystallization systems, including glutamic acid, glycine and, 3-nito-1,2,4-triazol-5-one (NTO), reported in the literature are analyzed as follows. Figure 2a

shows that the MSZW data of aqueous glutamic acid solutions fitted to linearized integral method I Equation (12) at various T_0, where the original experimental MSZW data listed in Table 1 are taken from Shiau and Lu [32] in a 200 mL vessel. The solubility of glutamic acid in water is taken as $C_{eq}(T) = 9.58654 \times 10^{-3}T^2 - 5.3778T + 759.067$; $C_{eq}\ in\ kg\ /m^3$,$T\ in\ K$ [37]. Note that $v = 1.674 \times 10^{-28}m^3$ for glutamic acid. Figure 2b shows the same MSZW data of aqueous glutamic acid solutions fitted to linearized integral method II Equation (14) at various T_0, where $\Delta H_d = 31.8\ kJ/mol$ is used for the van't Hoff solubility equation. For comparison, Figure 2c and Figure 2d show the same MSZW data of aqueous glutamic acid solutions fitted to the classical 3D approach Equation (19) and integral method Equation (4), respectively, at various T_0.

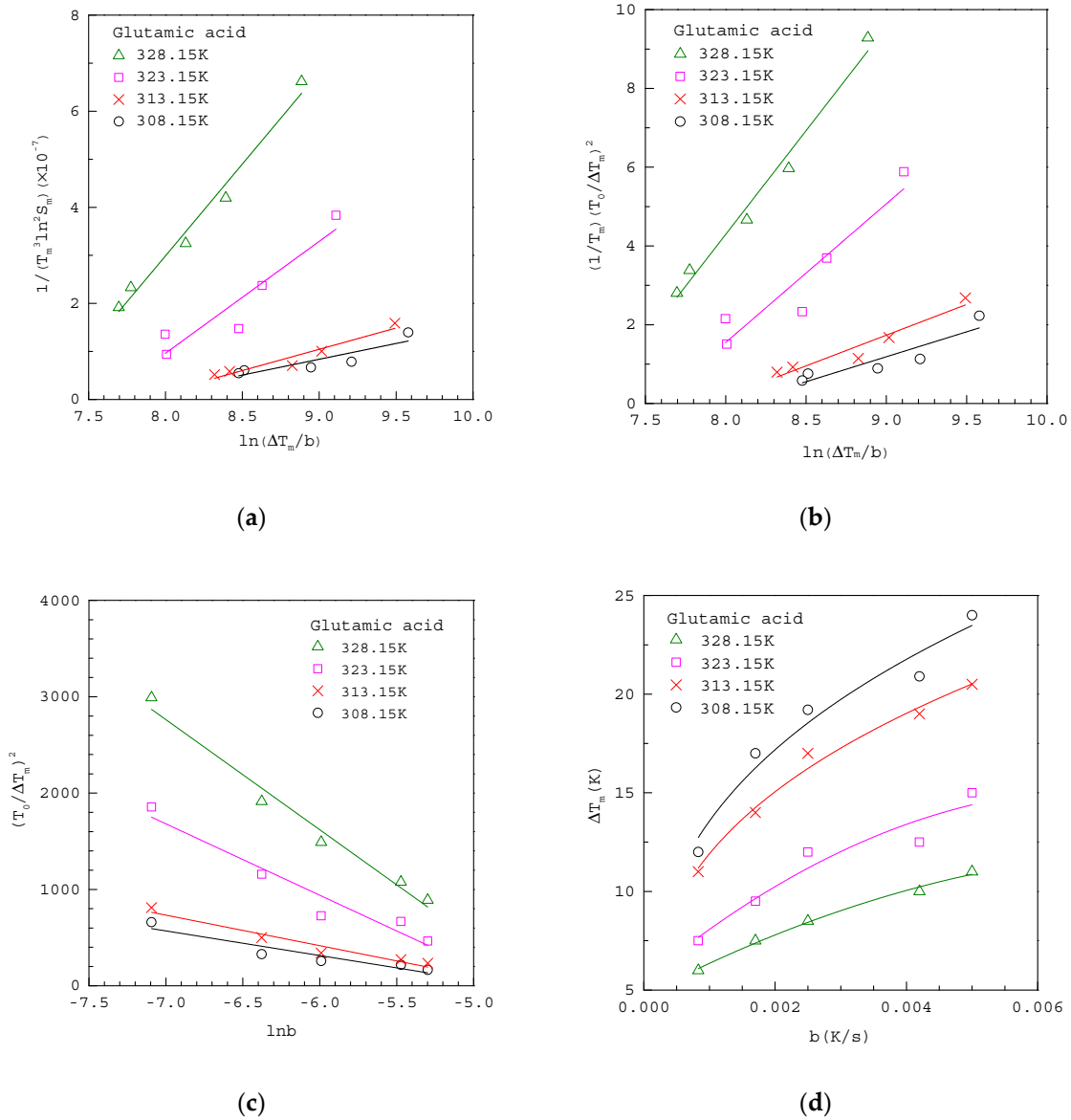

Figure 2. The experimental MSZW data of aqueous glutamic acid solutions at various T_0 (**a**) fitted to Equation (12); (**b**) fitted to Equation (14); (**c**) fitted to Equation (19); (**d**) fitted to Equation (4). The MSZW data are taken from Shiau and Lu [32].

Table 1. The experimental MSZW data of aqueous glutamic acid solutions taken from Shiau and Lu [32], where T_0 is the initial saturated temperature at the corresponding initial saturated concentration C_0.

$T_0(K)$	$C_0(kg/m^3)$	$\Delta T_m(K)$				
		$b = 0.00083\ K/s$	$b = 0.0017\ K/s$	$b = 0.0025\ K/s$	$b = 0.0042\ K/s$	$b = 0.005\ K/s$
308.15	12.2	12	17	19.2	20.9	24
313.15	15.1	11	14	17	19	20.5
323.15	22.3	7.5	9.5	12	12.5	15
328.15	26.6	6.0	7.5	8.5	10	11

Figure 3a shows that the MSZW data of aqueous glycine solutions fitted to linearized integral method I Equation (12) at various T_0, where the original experimental MSZW data listed in Table 2 are taken from Shiau [38] in a 200 mL vessel. The solubility of glycine in water is taken as $C_{eq}(T) = 5.4397 \times 10^{-3}T^2 - 3.2022 \times 10^{-1}T - 188.2$; $C_{eq}\ in\ kg\ /m^3, T\ in\ K$ [39]. Note that $v = 7.76 \times 10^{-29}m^3$ for glycine. Figure 3b shows the same MSZW data of aqueous glycine solutions fitted to linearized integral method II Equation (14) at various T_0, where $\Delta H_d = 10.2\ kJ/mol$ is used for the van't Hoff solubility equation. For comparison, Figure 3c and Figure 3d show the same MSZW data of aqueous glycine solutions fitted to classical 3D approach Equation (19) and integral method Equation (4), respectively, at various T_0.

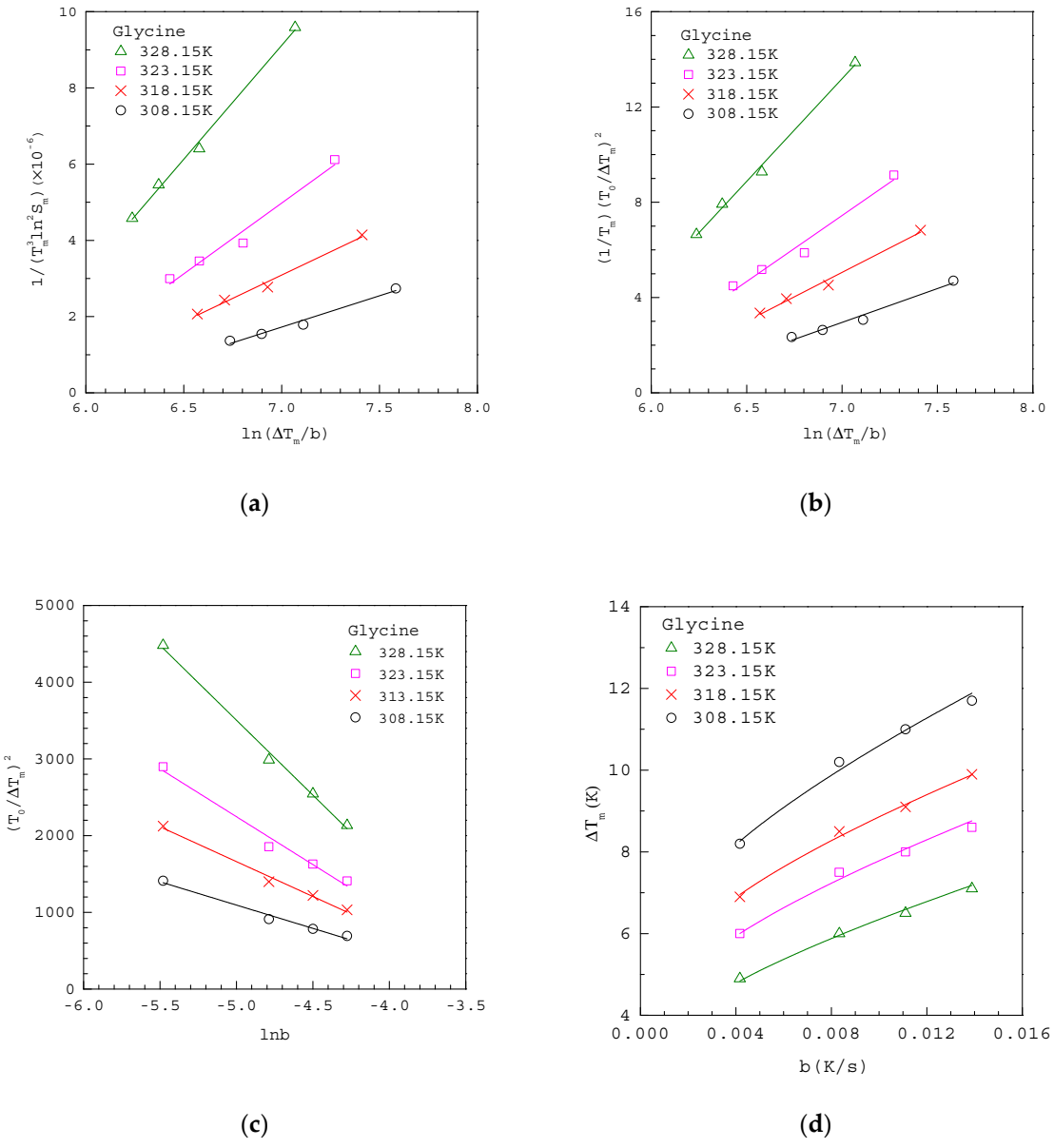

Figure 3. The experimental MSZW data of aqueous glycine solutions at various T_0 (**a**) fitted to Equation (12); (**b**) fitted to Equation (14); (**c**) fitted to Equation (19); (**d**) fitted to Equation (4). The MSZW data are taken from Shiau [38].

Table 2. The experimental MSZW data of aqueous glycine solutions taken from Shiau [38], where T_0 is the initial saturated temperature at the corresponding initial saturated concentration C_0.

$\boldsymbol{T_0(K)}$	$\boldsymbol{C_0(kg/m^3)}$	$\boldsymbol{\Delta T_m(K)}$			
		$\boldsymbol{b = 0.000417\ K/s}$	$\boldsymbol{b = 0.00833\ K/s}$	$\boldsymbol{b = 0.01111\ K/s}$	$\boldsymbol{b = 0.01389\ K/s}$
308.15	230	8.2	10.2	11	11.7
318.15	261	6.9	8.5	9.1	9.9
323.15	276	6.0	7.5	8.0	8.6
328.15	292	4.9	6.0	6.5	7.1

Figure 4a shows that the MSZW data of aqueous NTO solutions fitted to linearized integral method I Equation (12) at various T_0, where the original experimental MSZW data listed in Table 3 are taken from Kim et al. [40] in a 300 mL vessel. The solubility of NTO in water is taken as $C_{eq}(T) = 0.0153T^2 - 8.7002T - 1247.2$; $C_{eq}\ in\ kg\ /m^3$, $T\ in\ K$ [40]. Note that $v = 8.86 \times 10^{-29} m^3$ for NTO. Figure 4b shows the same MSZW data of aqueous NTO solutions fitted to linearized integral method II Equation (14) at various T_0, where $\Delta H_d = 26.1\ kJ/mol$ is used for the van't Hoff solubility equation. For comparison, Figure 4c and Figure 4d show the same MSZW data of aqueous NTO solutions fitted to the classical 3D approach Equation (19) and integral method Equation (4), respectively, at various T_0.

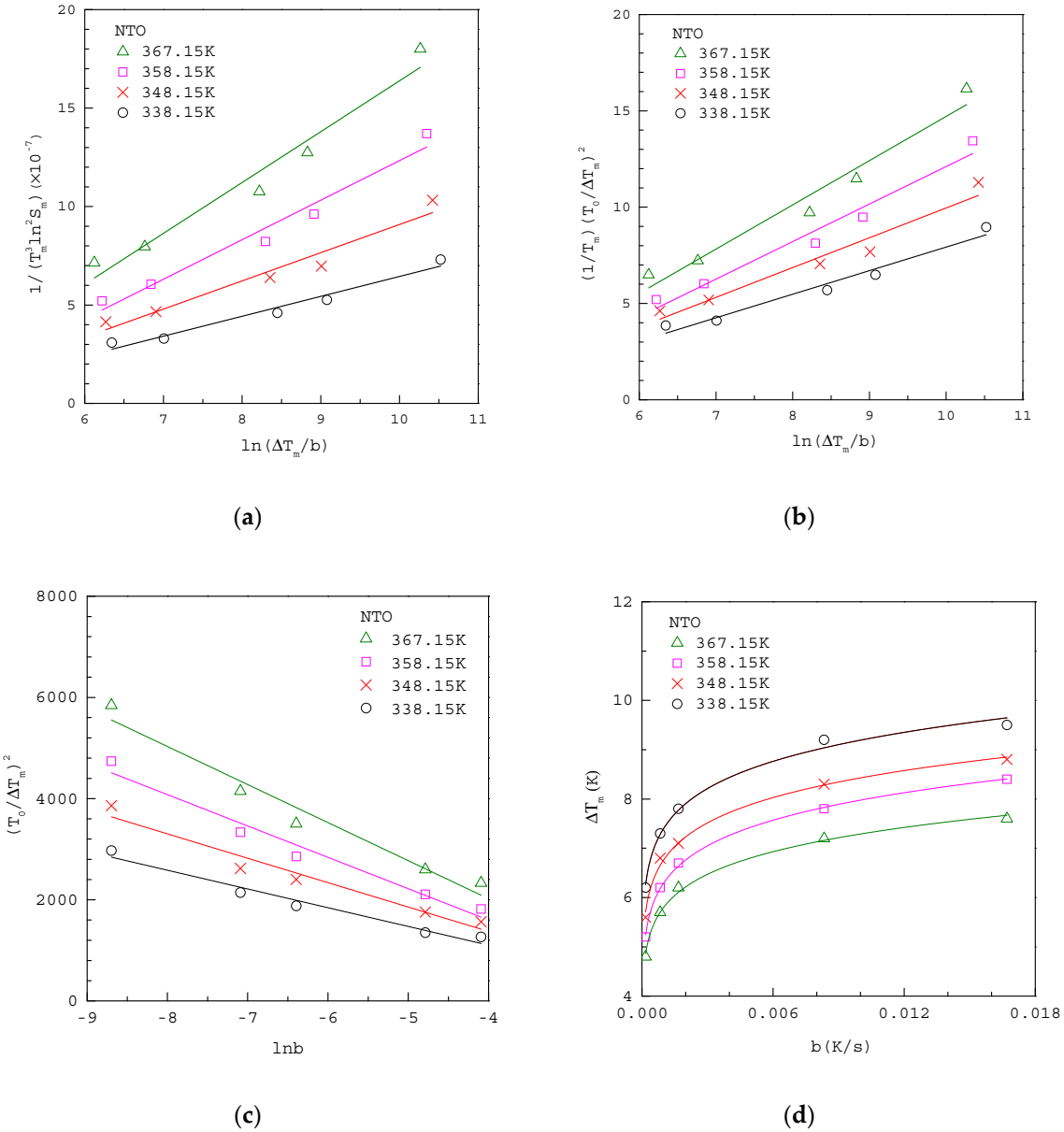

Figure 4. The experimental MSZW data of aqueous NTO solutions at various T_0 (**a**) fitted to Equation (12); (**b**) fitted to Equation (14); (**c**) fitted to Equation (19); (**d**) fitted to Equation (4). The MSZW data are taken from Kim et al. [40].

Table 3. The experimental MSZW data of aqueous NTO solutions taken from Kim et al. [40], where T_0 is the initial saturated temperature at the corresponding initial saturated concentration C_0.

$\boldsymbol{T_0(K)}$	$\boldsymbol{C_0(kg/m^3)}$	$\boldsymbol{\Delta T_m(K)}$				
		$\boldsymbol{b = 0.000167\ K/s}$	$\boldsymbol{b = 0.000833\ K/s}$	$\boldsymbol{b = 0.00167\ K/s}$	$\boldsymbol{b = 0.00833\ K/s}$	$\boldsymbol{b = 0.0167\ K/s}$
338.15	54.7	6.2	7.3	7.8	9.2	9.5
348.15	72.7	5.6	6.8	7.1	8.3	8.8
358.15	93.8	5.2	6.2	6.7	7.8	8.4
367.15	115.4	4.8	5.7	6.2	7.2	7.6

The fitted results for glutamic acid, glycine, and NTO are listed in Tables 4–6. As integral method Equation (4) is numerically integrated without any approximations in this study, γ and $\frac{A_J}{f_N}$ obtained from integral method Equation (4) represent the exact solution to Equation (2) based on the nucleation event assumed corresponding to a point at which the total number density of the nuclei has reached f_N. For all three studied systems, as opposed to γ obtained from classical 3D approach Equation (19) compared with that obtained from integral method Equation (4), γ obtained from linearized integral methods Equations (12) and (14) is closer to that obtained from integral method Equation (4) at each condition. Furthermore, $\frac{A_J}{f_N}$ obtained from linearized integral methods Equations (12) and (14) is also consistent with that obtained from integral method Equation (4) at each condition. As f_N and f are two different parameters, A_J determined from Equations (4), (12) and (14) based on $f_N = 7.64 \times 10^{11}\ m^{-3}$ is not strictly comparable with that determined from Equation (19) based on $f = 10^{27}\ m^{-3}$. It should be noted in Tables 4–6 that γ and $\frac{A_J}{f_N}$ (or $\frac{A_J}{f}$) are determined first without the knowledge of f_N (or f). Consequently, γ is not influenced by the chosen value of f_N (or f) although A_J needs to be determined based on f_N (or f). For example, if the chosen value of f_N (or f) is increased by ten times, A_J is also increased by ten times at each condition while γ remains unchanged.

Table 4. The fitted results of γ and A_J at various T_0 for aqueous glutamic acid solution based on $f_N = 7.64 \times 10^{11}\ m^{-3}$ and $f = 10^{27}\ m^{-3}$.

$T_0(K)$	Linearized Integral Method I Equation (12)				Linearized Integral Method II Equation (14)			
	$\gamma(mJ/m^2)$	$\frac{A_J}{f_N}(s^{-1})$	$A_J(m^{-3}s^{-1})$	$R^2(-)$	$\gamma(mJ/m^2)$	$\frac{A_J}{f_N}(s^{-1})$	$A_J(m^{-3}s^{-1})$	$R^2(-)$
308.15	4.4	8.84×10^{-4}	6.76×10^{8}	0.797	4.0	6.30×10^{-4}	4.81×10^{8}	0.829
313.15	4.0	8.05×10^{-4}	6.15×10^{8}	0.924	3.8	7.51×10^{-4}	5.73×10^{8}	0.930
323.15	2.9	1.01×10^{-3}	7.75×10^{8}	0.886	2.9	1.04×10^{-3}	7.96×10^{8}	0.887
328.15	2.5	1.47×10^{-3}	1.12×10^{9}	0.982	2.5	1.52×10^{-3}	1.16×10^{9}	0.983
$T_0(K)$	Integral Method Equation (4)				Classical 3D Approach Equation (19)			
	$\gamma(mJ/m^2)$	$\frac{A_J}{f_N}(s^{-1})$	$A_J(m^{-3}s^{-1})$	$CV(-)$	$\gamma(mJ/m^2)$	$\frac{A_J}{f}(s^{-1})$	$A_J(m^{-3}s^{-1})$	$R^2(-)$
308.15	3.2	5.06×10^{-4}	3.87×10^{8}	0.175	4.6	3.62×10^{-4}	3.62×10^{23}	0.893
313.15	3.1	6.27×10^{-4}	4.79×10^{8}	0.106	4.3	3.80×10^{-4}	3.80×10^{23}	0.949
323.15	2.2	7.91×10^{-4}	6.04×10^{8}	0.149	3.3	3.34×10^{-4}	3.34×10^{23}	0.939
328.15	2.0	1.35×10^{-3}	1.03×10^{9}	0.047	2.9	2.87×10^{-4}	2.87×10^{23}	0.979

Table 5. The fitted results of γ and A_J at various T_0 for aqueous glycine solutions based on $f_N = 7.64 \times 10^{11}\ m^{-3}$ and $f = 10^{27}\ m^{-3}$.

$T_0(K)$	Linearized Integral Method I Equation (12)				Linearized Integral Method II Equation (14)			
	$\gamma(mJ/m^2)$	$\frac{A_J}{f_N}(s^{-1})$	$A_J(m^{-3}s^{-1})$	$R^2(-)$	$\gamma(mJ/m^2)$	$\frac{A_J}{f_N}(s^{-1})$	$A_J(m^{-3}s^{-1})$	$R^2(-)$
308.15	2.5	5.21×10^{-3}	3.98×10^{9}	0.979	2.4	5.16×10^{-3}	3.95×10^{9}	0.980
318.15	2.2	6.46×10^{-3}	4.93×10^{9}	0.990	2.1	6.26×10^{-3}	4.78×10^{9}	0.989
323.15	1.9	6.97×10^{-3}	5.32×10^{9}	0.976	1.9	7.00×10^{-3}	5.34×10^{9}	0.976
328.15	1.6	8.38×10^{-3}	6.40×10^{9}	0.996	1.7	8.43×10^{-3}	6.44×10^{9}	0.996
$T_0(K)$	Integral Method Equation (4)				Classical 3D Approach Equation (19)			
	$\gamma(mJ/m^2)$	$\frac{A_J}{f_N}(s^{-1})$	$A_J(m^{-3}s^{-1})$	$CV(-)$	$\gamma(mJ/m^2)$	$\frac{A_J}{f}(s^{-1})$	$A_J(m^{-3}s^{-1})$	$R^2(-)$
308.15	2.0	4.95×10^{-3}	3.78×10^{9}	0.044	2.7	5.47×10^{-4}	5.47×10^{23}	0.983
318.15	1.8	6.25×10^{-3}	4.78×10^{9}	0.032	2.4	5.23×10^{-4}	5.23×10^{23}	0.990
323.15	1.6	6.73×10^{-3}	5.14×10^{9}	0.048	2.2	4.91×10^{-4}	4.91×10^{23}	0.981
328.15	1.4	8.22×10^{-3}	6.28×10^{9}	0.018	1.9	4.71×10^{-4}	4.71×10^{23}	0.995

Table 6. The fitted results of γ and A_J at various T_0 for aqueous NTO solutions based on $f_N = 7.64 \times 10^{11}\ m^{-3}$ and $f = 10^{27}\ m^{-3}$.

$T_0(K)$	Linearized Integral Method I Equation (12)	Linearized Integral Method II Equation (14)

	$\gamma(mJ/m^2)$	$\frac{A_J}{f_N}(s^{-1})$	$A_J(m^{-3}s^{-1})$	$R^2(-)$	$\gamma(mJ/m^2)$	$\frac{A_J}{f_N}(s^{-1})$	$A_J(m^{-3}s^{-1})$	$R^2(-)$
338.15	5.8	5.34×10^{-2}	4.08×10^{10}	0.967	5.4	5.89×10^{-2}	4.50×10^{10}	0.967
348.15	5.2	5.18×10^{-2}	3.96×10^{10}	0.952	5.0	5.67×10^{-2}	4.33×10^{10}	0.952
358.15	4.6	4.22×10^{-2}	3.22×10^{10}	0.968	4.7	4.54×10^{-2}	3.47×10^{10}	0.968
367.15	4.3	5.18×10^{-2}	3.96×10^{10}	0.962	4.4	5.52×10^{-2}	4.22×10^{10}	0.962
$T_0(K)$	**Integral Method Equation (4)**				**Classical 3D Approach Equation (19)**			
	$\gamma(mJ/m^2)$	$\frac{A_J}{f_N}(s^{-1})$	$A_J(m^{-3}s^{-1})$	$CV(-)$	$\gamma(mJ/m^2)$	$\frac{A_J}{f}(s^{-1})$	$A_J(m^{-3}s^{-1})$	$R^2(-)$
338.15	5.5	1.17×10^{-1}	8.94×10^{10}	0.284	5.6	1.01×10^{-2}	1.01×10^{25}	0.969
348.15	4.8	9.43×10^{-2}	7.2×10^{10}	0.309	5.2	8.37×10^{-3}	8.37×10^{24}	0.955
358.15	4.3	8.04×10^{-2}	6.14×10^{10}	0.250	4.8	6.03×10^{-3}	6.03×10^{24}	0.969
367.15	4.0	1.04×10^{-1}	7.95×10^{10}	0.286	4.6	6.37×10^{-3}	6.37×10^{24}	0.964

As compared in Tables 4–6, γ and A_J obtained from linearized integral method I Equation (12) are consistent with those obtained from linearized integral method II Equation (14) at each condition for all three studied systems. Thus, both equations can be applied to determine γ and A_J of the crystallized substance using the MSZW data. As opposed to the temperature-dependent solubility required for linearized integral method I Equation (12), only the value of ΔH_d is required in application of linearized integral method II Equation (14).

4. Conclusions

A linear regression method is proposed in this work to determine the pre-exponential factor and interfacial energy based on CNT using the MSZW data. Linearized integral method I Equation (12) is derived for any temperature-dependent functional form of the solubility while linearized integral method II Equation (14) is derived for the van't Hoff temperature-dependent solubility. Only the value of ΔH_d is required in application of linearized integral method II Equation (14), as opposed to the temperature-dependent solubility required for linearized integral method I Equation (12). The experimental MSZW data for all three studied systems, including glutamic acid, glycine, and NTO, are fitted well to these two equations. The pre-exponential factor and interfacial energy obtained from linearized integral method I Equation (12) are consistent with those obtained from linearized integral method II Equation (14) for these systems.

As the integral method is numerically integrated without any approximations, the pre-exponential factor and interfacial energy obtained from the integral method represent the exact values based on the nucleation event assumed corresponding to a point at which the total number density of the nuclei has reached a fixed value. As opposed to the interfacial energy obtained from classical 3D nucleation theory approach compared with that from the integral method, the interfacial energy obtained from linearized integral methods Equations (12) and (14) is closer to that from the integral method at each condition. Furthermore, the pre-exponential factor obtained from linearized integral method Equations (12) and (14) is also consistent with that from the integral method at each condition.

Funding: The author would like to thank Chang Gung Memorial Hospital (CMRPD2G0242) and the Ministry of Science and Technology of Taiwan (MOST108-2221-E-182-034) for financial support of this research.

Conflicts of Interest: The author declares no conflict of interest.

Notation

A_J = nucleation pre-exponential factor $(m^{-3}s^{-1})$
b = cooling rate (K/s)
C_0 = initial saturated concentration of solutes at T_0 (kg/m^3)
C_{eq} = saturated concentration of solutes (kg/m^3)
f = number of clusters per unit volume (m^{-3})
f_N = minimum detectable number density of generated nuclei (m^{-3})
f_V = minimum detectable volume fraction of generated nuclei $(-)$
J = nucleation rate $(m^{-3}s^{-1})$
J_0 = nucleation rate at $t = 0$ $(m^{-3}s^{-1})$
J_m = nucleation rate at t_m $(m^{-3}s^{-1})$
k_B = Boltzmann constant $(= 1.38 \times 10^{-23}\ J/K)$
k_V = volume shape factor $(-)$
M_W = molar mass (kg/mol)
N_A = Avogadro number $(= 6.02 \times 10^{23}\ mol^{-1})$
R_G = gas constant $(= 8.314\ J\ mol^{-1}K^{-1})$
S = supersaturation ratio $(-)$
S_m = supersaturation ratio at t_m $(-)$
T = temperature (K)
T_0 = initial saturated temperature (K)

T_m = temperature at t_m (K)
t = time (s)
t_i = induction time (s)
t_m = time at the MSZW limit (s)

Greek letters

ρ_C = crystal density (kg/m^3)
v = volume of the solute molecule (m^3)
γ = surface energy $(J\ m^{-2})$
ΔH_d = heat of dissolution $(J\ mol^{-1})$
ΔT_m = MSZW (K)

References

1. Mullin, J.W. *Crystallization*; Butterworth-Heinemann: Oxford, UK, 1993.
2. Kashchiev, D. *Nucleation: Basic Theory with Applications*; Butterworth-Heinemann: Oxford, UK, 2000.
3. Kashchiev, D.; van Rosmalen, G.M. Review: Nucleation in solutions revisited. *Cryst. Res. Technol.* **2003**, *38*, 555–574.
4. Sohnel, O.; Mullin, J.W. A method for the determination of precipitation induction periods. *J. Cryst. Growth* **1978**, *44*, 377–382.
5. Lancia, A.; Musmarra, D.; Prisciandaro, M. Measuring induction period for calcium sulfate dihydrate precipitation. *AIChE J.* **1999**, *45*, 390–396.
6. Granberg, R.A.; Ducreux, C.; Gracin, S.; Rasmuson, A.C. Primary nucleation of paracetamol in acetone–water mixtures. *Chem. Eng. Sci.* **2001**, *56*, 2305–2313.
7. Omar, W.; Mohnicke, M.; Ulrich, J. Determination of the solid liquid interfacial energy and thereby the critical nucleus size of paracetamol in different solvents. *Cryst. Res. Technol.* **2006**, *41*, 337–343.
8. Yang, H.; Rasmuson, A.C. Nucleation of butyl paraben in different solvents. *Cryst. Growth Des.* **2013**, *13*, 4226–4238.
9. You, S.; Zhang, Y.; Zhang, Y. Nucleation of ammonium aluminum sulfate dodecahydrate from unseeded aqueous solution. *J. Cryst. Growth* **2015**, *411*, 24–29.
10. Du, G.; Sun, Z.; Xian, Y.; Jing, H.; Chen, H.; Yin, D. The nucleation kinetics of ammonium metavanadate precipitated by ammonium chloride. *J. Cryst. Growth* **2016**, *441*, 117–123.
11. Nyvlt, J. Kinetics of crystallization in solution. *J. Cryst. Growth* **1968**, *3/4*, 377–383.
12. Nyvlt, J.; Sohnel, O.; Matuchova, M.; Broul, M. *The Kinetics of Industrial Crystallization*; Academia: Prague, Czech Republic, 1985.
13. Sangwal, K. A novel self-consistent Nyvlt-like equation for metastable zone width determined by the polythermal method. *Cryst. Res. Technol.* **2009**, *44*, 231–247.
14. Sangwal, K. New approach to analyze metastable zone width determined by the polythermal method: Physical interpretation of various parameters. *Cryst. Growth Des.* **2009**, *9*, 942–950.
15. Sangwal, K. Effects of impurities on the metastable zone width of solute-solvent systems. *J. Cryst. Growth* **2009**, *311*, 4050–4061.
16. Sangwal, K. On the effects of impurities on the metastable zone width of phosphoric acid. *J. Cryst. Growth* **2010**, *312*, 3316–3325.
17. Kashchiev, D.A.; Borissova, A.; Hammond, R.B.; Roberts, K.J. Effect of cooling rate on the critical undercooling for crystallization. *J. Cryst. Growth* **2010**, *312*, 698–704.
18. Kashchiev, D.A.; Borissova, A.; Hammond, R.B.; Roberts, K.J. Dependence of the critical undercooling for crystallization on the cooling rate. *J. Phys. Chem.* **2010**, *114*, 5441–5446.
19. Kubota, N. A new interpretation of metastable zone widths measured for unseeded solutions. *J. Cryst. Growth* **2008**, *310*, 629–634.
20. Zhang, X.; Qian, G.; Zhou, X. Effects of different organic acids on solubility and metastable zone width of zinc lactate. *J. Chem. Eng. Data* **2012**, *57*, 2963–2970.
21. Peng, J.; Dong, Y.; Wang, L.; Li, L.; Li, W.; Feng, H. Effect of impurities on the solubility, metastable zone width, and nucleation kinetics of borax decahydrate. *Ind. Eng. Chem. Res.* **2014**, *53*, 12170–12178.

22. Zhang, X.; Yang, Z.; Chai, J.; Xu, J.; Zhang, Z.; Qian, G.; Zhou, X. Nucleation kinetics of lovastatin in different solvents from metastable zone widths. *Chem. Eng. Sci.* **2015**, *133*, 62–69.
23. Jiang, X.; Ruan, X.; Xiao, W.; Lu, D.; He, G. A novel membrane distillation response technology for nucleation detection, metastable zone width measurement and analysis. *Chem. Eng. Sci.* **2015**, *134*, 671–680.
24. Wang, L.; Feng, H.; Dong, Y.; Peng, J.; Li, W. Solubility and metastable zone width of aqueous sodium dichromate dehydrate solutions in the presence of sodium chromate additive. *J. Cryst. Growth* **2016**, *454*, 105–110.
25. Luo, M.; Liu, C.; Xue, J.; Li, P.; Yu, J. Determination of metastable zone width of potassium sulfate in aqueous solution by ultrasonic sensor and FBRM. *J. Cryst. Growth* **2017**, *469*, 144–153.
26. Zhou, L.; Wang, Z.; Zhang, M.; Guo, M.; Xu, S.; Yin, Q. Determination of metastable zone and induction time of analgin for cooling crystallization. *Chin. J. Chem. Eng.* **2017**, *25*, 313–318.
27. Mastan, T.H.; Lenka, M.; Sarkar, D. Nucleation kinetics from metastable zone widths for sonocrystallization of L-phenylalanine. *Ultrason. Sonochem.* **2017**, *36*, 497–506.
28. Xu, S.; Wang, J.; Zhang, K.; Wu, S.; Li, S.; Li, K.; Yu, B.; Gong, J. Nucleation behavior of eszopiclone-butyl acetate solutions from metastable zone widths. *Chem. Eng. Sci.* **2016**, *155*, 248–257.
29. Huang, Y.; Lu, J.; Chen, H.; Du, W.; Wang, X. Effects of succinic acid and adipic acid on the metastable width of glutaric acid in acetic acid. *J. Cryst. Growth* **2019**, *507*, 1–9.
30. Chen, J.; Peng, J.; Wang, X.; Dong, Y.; Li, W. Effects of CO_3^{2-} and OH^- on the solubility, metastable zone width and nucleation kinetics of borax decahydrate. *R. Soc. Open Sci.* **2019**, *6*, 181862.
31. Shiau, L.D.; Lu, T.S. A model for determination of the interfacial energy from the measured metastable zone width data by the polythermal method. *J. Cryst. Growth* **2014**, *402*, 267–272.
32. Shiau, L.D.; Lu, T.S. A model for determination of the interfacial energy from the induction time or metastable zone width data based on turbidity measurements. *CrystEngComm*. **2014**, *16*, 9743–9752.
33. Shiau, L.D. Comparison of the interfacial energy and pre-exponential factor calculated from the induction time and metastable zone width data based on classical nucleation theory. *J. Cryst. Growth* **2016**, *450*, 50–55.
34. Mersmann, A.; Bartosch, K. How to predict the metastable zone width. *J. Cryst. Growth* **1998**, *183*, 240–250.
35. Lindenberg, C.; Mazzotti, M. Effect of temperature on the nucleation kinetics of α L-glutamic acid. *J. Cryst. Growth* **2009**, *311*, 1178–1184.
36. Shiau, L.D. Determination of the nucleation and growth kinetics from aqueous L-glycine solutions from the turbidity induction time data. *Crystals* **2018**, *8*, 403.
37. Emanuel, M.; Alexander, A. Solubilities of L-glutamic acid, 3-nitrobenzoic acid, p-toluic acid, calcium-L-lactate, calcium gluconate, magnesium-DL-aspartate, and magnesium-L-lactate in water. *J. Chem. Thermodyn.* **2002**, *34*, 1127–1136.
38. Shiau, L.D. The temperature dependence of the pre-exponential factor and interfacial energy for aqueous glycine solutions based on the metastable zone width data. *J. Cryst. Growth* **2018**, *496–497*, 18–23.
39. Park, K.; Evans, J.M.B.; Myerson, A.S. Determination of solubility of polymorphs using differential scanning calorimetry. *Cryst. Growth Des.* **2003**, *3*, 991–995.
40. Kim, K.J.; Kim, M.J.; Lee, J.M.; Kim, S.H.; Kim, H.S.; Park, B.S. Solubility, density, and metastable zone width of the 3-nito-1,2,4-triazol-5-one + water system. *J. Chem. Eng. Data* **1998**, *43*, 65–68.